*Sensors and Materials*, Vol. 34, No. 5 (2022) 1779–1789
MYU Tokyo



S & M 2928

# Adaptive Speed Prediction for Direct Torque-controlled Permanent Magnet Synchronous Motor Drive Using Elephant Herding Optimization Algorithm

Yung-Chang Luo,* Yan-Xun Peng, Chia-Hung Lin, and Ying-Piao Kuo

Department of Electrical Engineering, National Chin-Yi University of Technology,
No. 57, Sec. 2, Zhongshan Rd, Taiping Dist, Taichung 41170, Taiwan (ROC)

(Received November 25, 2021; accepted February 28, 2022)

***Keywords:*** direct torque-controlled (DTC) permanent magnet synchronous motor (PMSM) drive, speed prediction, model reference adaptive control (MRAC), elephant herding optimization (EHO) algorithm

In this study, an adaptive speed prediction scheme based on reactive power was established for direct torque-controlled (DTC) permanent magnet synchronous motor (PMSM) drives. The current and flux of a stator were used to establish a DTC PMSM drive. Hall effect current sensors with a non-contact sensing technique were used to detect the stator current of the PMSM. The voltage space vector pulse width modulation (VSVPWM) DTC scheme was used in place of a traditional switching table (ST) DTC scheme to reduce current and torque ripples. Model reference adaptive control (MRAC) was utilized to develop a speed prediction scheme, and its adaptation mechanism was designed using the elephant herding optimization (EHO) algorithm. The torque, flux, and speed controllers were designed using a proportional–integral (P–I)-type controller. The MATLAB/Simulink© toolbox was used to establish the simulation scheme, and all control algorithms were realized using a microprocessor control card. The simulation and experimental results confirmed the effectiveness of the proposed approach.

## 1. Introduction

The development of the green energy automation industry requires many intelligent and high-efficiency apparatuses. The permanent magnet synchronous motor (PMSM) uses high-permeability permanent magnets as the rotor magnetic field, which makes PMSM drives suitable for actuating energy-saving precision machines. Compared with the conventional field-orientation-controlled based scheme, the direct torque-controlled (DTC) based scheme can directly control the flux and torque independently, and also exhibits a simple structure, without decoupling computation, and attains quick responses. In traditional switching table (ST) DTC PMSM drives, the stator flux and torque are directly dominated by two-level and three-level hystereses, respectively, and the suitable switching patterns of the voltage source inverter (VSI) are selected to actuate the motor.(1) The band–band-type hysteresis obtains quick responses and is easy to design. However, the torque and current ripples are notable, and the non-fixed

*Corresponding author: e-mail: luoyc@ncut.edu.tw
https://doi.org/10.18494/SAM3748

ISSN 0914-4935 

switching frequency causing the filter is difficult to design. In voltage space vector pulse width modulation (VSVPWM) DTC drives, a VSVPWM VSI is used in place of ST VSI, and the flux and torque hystereses of the ST DTC scheme are replaced by a proportional–integral (P–I)-type controller. Conventional speed control DTC PMSM drives require a digital encoder to detect shaft positions. However, this sensor diminishes the robustness of PMSM drives. Hence, the development of speed prediction methods for DTC PMSM drives in place of the conventional speed feedback scheme is imperative. Numerous speed prediction methods of DTC PMSM drives have been proposed; examples of such prediction methods are speed identification utilizing the back electromotive of PMSM,[2,3] speed determination derived from a flux observer or estimator,[4–6] speed estimation using fuzzy logic control or chaos theory,[7–9] speed identification using high-frequency signal injection,[10–12] and speed adjustment dependent on adaptive control approaches.[13–15] In this research, a VSVPWM VSI scheme was established for DTC PMSM drives in place of the traditional ST VSI scheme to reduce torque and current ripples. The development of a speed prediction method for DTC PMSM drives used the model reference adaptive control (MRAC) based on the reactive power, and the adaptation mechanism of the MRAC was designed using the elephant herding optimization (EHO) algorithm. Hall effect currents were used to measure the current for the implementation of the MRAC speed prediction.[16]

This paper is presented in six sections. Section 1 presents the research motivation, background, and literature review on speed prediction methods for DTC PMSM drives. Section 2 describes the DTC PMSM drive based on the VSVPWM VSI scheme and compares it with the ST VSI scheme. Section 3 develops the MRAC speed prediction method based on the reactive power of the PMSM. Section 4 details the design of the adaptation mechanism of MRAC using the EHO algorithm. Sections 5 and 6 cover the experimental setup and results, discussion, and conclusions.

## 2. DTC PMSM Drives

In a surface-mounted-magnet rotor without damping winding, the permanent magnet's axis coincides with the *d*-axis component of the rotor shaft. The *d*-axis and *q*-axis stator voltage equations of the PMSM in the synchronous reference coordinate frame are given by [17]

$$(R_s + L_s p) i_{ds}^e - \omega_e L_s i_{qs}^e = v_{ds}^e , \tag{1}$$

$$(R_s + L_s p) i_{qs}^e + \omega_e L_s i_{ds}^e + \omega_e \lambda_F = v_{qs}^e , \tag{2}$$

where $i_{ds}^e$ and $i_{qs}^e$ are the *d*-axis and *q*-axis stator currents; $v_{ds}^e$ and $v_{qs}^e$ are the *d*-axis and *q*-axis stator voltages; $R_s$ and $L_s$ are the resistance and inductance of the stator, respectively; $\lambda_F$ is the equivalent rotor flux linkage produced by the permanent magnets of the rotor; $\omega_e$ is the speed of the synchronous reference coordinate frame; and $p = d/dt$ is the differential operator.

Under a DTC condition, the estimated *d*-axis and *q*-axis stator fluxes in the stationary reference coordinate ($\omega_e = 0$) frame are

$$\hat{\lambda}_{ds}^{s} = \frac{\tau_c}{1+s\tau_c}(v_{ds}^{s} - R_s i_{ds}^{s}) + \frac{1}{1+s\tau_c}\lambda_{ds}^{s\,*}, \tag{3}$$

$$\hat{\lambda}_{qs}^{s} = \frac{\tau_c}{1+s\tau_c}(v_{qs}^{s} - R_s i_{qs}^{s}) + \frac{1}{1+s\tau_c}\lambda_{qs}^{s\,*}, \tag{4}$$

where the symbol ^ stands for the estimated value, $s$ is the Laplace operator, $\tau_c$ is the time constant of the low-pass filter, and $\lambda_{ds}^{s\,*}$ and $\lambda_{qs}^{s\,*}$ are the *d*-axis and *q*-axis components of the stator flux reference, respectively.

By utilizing Eqs. (3) and (4), the estimated synchronous position angle for the implementation of the traditional DTC strategy is obtained from

$$\hat{\theta}_e = \tan^{-1}\left(\frac{\hat{\lambda}_{qs}^{s}}{\hat{\lambda}_{ds}^{s}}\right). \tag{5}$$

The developed electromagnetic torque of the PMSM under a DTC condition is given by

$$T_e = \frac{3P}{4}(i_{qs}^{s}\hat{\lambda}_{ds}^{s} - i_{ds}^{s}\hat{\lambda}_{qs}^{s}), \tag{6}$$

where $P$ is the number of motor poles. The mechanical equation of the PMSM is acquired as

$$T_L + B_m\omega_{rm} + J_m p\omega_{rm} = T_e, \tag{7}$$

where $T_L$ is the load torque; $B_m$ and $J_m$ are the viscous friction coefficient and inertia of the motor, respectively; $\omega_{rm} = (2/P)\omega_r$ is the mechanical speed of the motor shaft; and $\omega_r$ is the electric speed of the rotor.

### 2.1 ST DTC scheme

A block diagram of the traditional ST VSI closed-loop DTC PMSM drive is shown in Fig. 1, which includes a speed controller, three-level torque hysteresis, two-level flux hysteresis, voltage vector ST, sector detection, switching-state to stator-voltage calculation, torque calculation, stator flux and flux position angle calculation, and three-phase stationary to two-axis stationary coordinate transformation ($3^s \Rightarrow 2^s$).

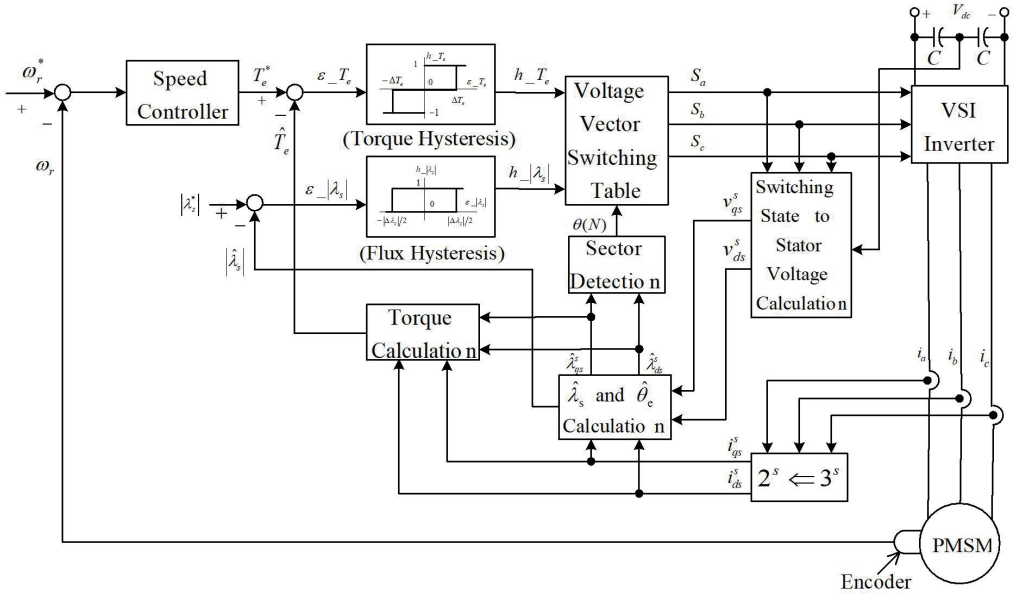


Fig. 1. Traditional ST VSI closed-loop DTC PMSM drive.

### 2.2 VSVPWM DTC scheme

A block diagram of the conventional VSVPWM VSI closed-loop DTC PMSM drive is shown in Fig. 2, which includes a speed controller, torque controller, flux controller, VSVPWM, torque calculation, stator flux and flux position angle calculation, and three-phase stationary to two-axis stationary coordinate transformation ($3^s$ => $2^s$).

The total harmonic distortions (THDs, %) of the traditional ST VSI (19.44%) and conventional VSVPWM VSI (9.09%) closed-loop DTC PMSM drives are shown in Figs. 3(a) and 3(b), respectively. Here, the THD % of the conventional VSVPWM closed-loop DTC PMSM drive is less than those of the traditional ST VSI ones.

## 3. MRAC Speed Prediction Based on Reactive Power of PMSM

In the proposed DTC PMSM drive, the rotor speed feedback signal was replaced with a predicted rotor speed. This predicted rotor speed was derived from the developed MRAC speed prediction scheme based on the reactive power.

The reactive power of a PMSM obtained from the power source in the synchronous reference coordinate frame is given by

$$Q = v_{qs}^e i_{ds}^e - v_{ds}^e i_{qs}^e . \tag{8}$$

Under the DTC condition, by substituting Eqs. (1) and (2) into Eq. (8), the reactive power of a PMSM can also be expressed as

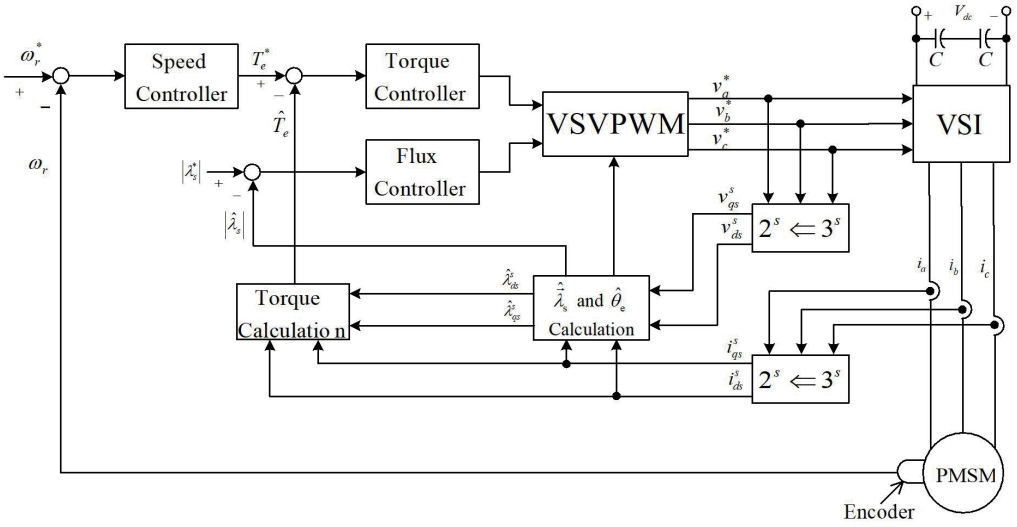


Fig. 2. Conventional VSVPWM VSI closed-loop DTC PMSM drive.

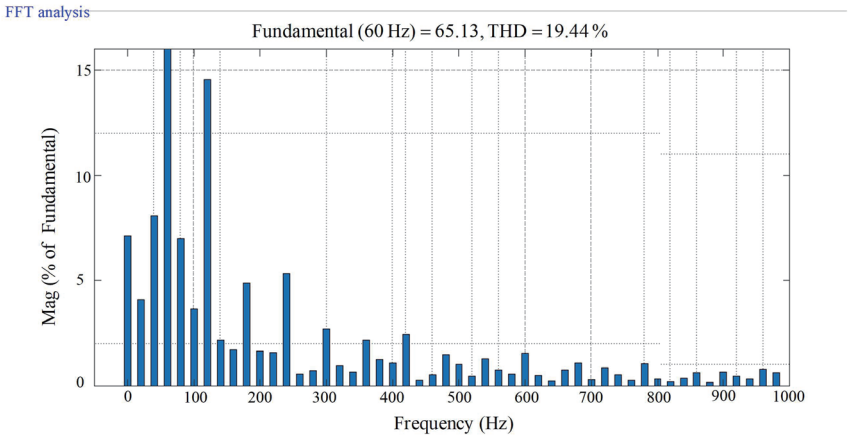


(a)

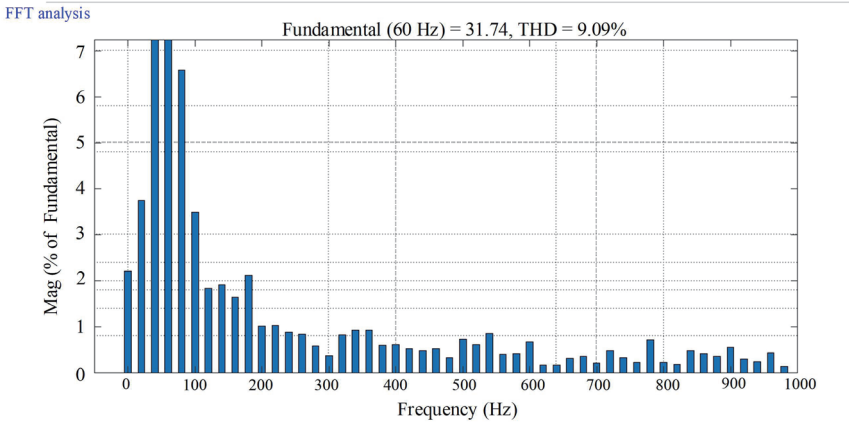


(b)

Fig. 3. (Color online) THD % for (a) ST VSI and (b) VSVPWM VSI.

$$Q' = \hat{\omega}_e[L_s(i_{ds}^e)^2 + L_s(i_{qs}^e)^2 + \lambda_F i_{ds}^e]. \tag{9}$$

On the basis of the MRAC theory,[18] Eq. (8) was selected as the reference model because it does not involve the estimated synchronous speed $\hat{\omega}_e$, whereas Eq. (7) contains $\hat{\omega}_e$, which was selected as the adjustable model. The difference between the reference model and the adjustable model was determined through an adaptation mechanism to identify $\hat{\omega}_e$. The developed MRAC predicted synchronous speed scheme is shown in Fig. 4. Here, the estimated synchronous position angle $\hat{\theta}_e$ for the implementation of a VSVPWM and the coordinate transformation from the two-axis synchronous frame to the two-axis stationary frame ($2^s$ => $2^e$) is given by

$$\hat{\theta}_e = \int \hat{\omega}_e dt. \tag{10}$$

## 4. Adaptation Mechanism Design Using EHO Algorithm

The EHO algorithm was used to design the adaptation mechanism of the MRAC rotor speed prediction scheme based on the reactive power. It is a swarm intelligence optimization algorithm,[19–21] derived from the animal husbandry behavior of elephants in nature, and is used to solve global unconstrained optimization problems. The EHO algorithm is a heuristic algorithm that can easily solve optimization problems. It has a simple structure and few control parameters, and can easily be combined with other methods.

In nature, an elephant herd can be divided into several clans, and each clan has a female elephant as its leader. In each generation, a certain number of male elephants will leave the clan. The elephants of different clans all live under the leadership of the patriarch (the best elephant in the clan). A fixed number of male elephants will leave their clan after they mature and then perform a clan update to change the position of each elephant in the new clan. After the elephant

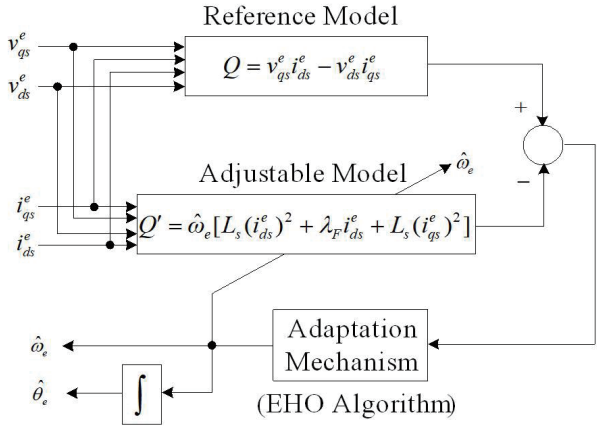


Fig. 4. MRAC rotor speed prediction scheme based on reactive power.

obtains the position of the new clan, a classification operation is performed to optimize the elephant with a poor position in the clan.

In the basic EHO algorithm, the clan represents a local search, and the male elephants leaving the clan perform a global search. First, the update operation is performed to determine the search direction of the algorithm and the detailed local search level, and then the separation operation is performed. The basic EHO consists of clan update and clan separation operations.

### 4.1 Clan update operation

Elephants from different herds will live together under the leadership of the patriarch. The matriarch has the best fitness in the elephant clan. Each elephant will update its position according to the corresponding position relationship with the matriarch and update the position of the patriarch on the basis of the central position of the clan.

Here, we randomly initialized the elephant population and divided the elephant herd into $n$ clans. Accordingly, there are $j$ individual elephants in each clan. In each iteration, the position $j$ of each individual elephant will move with the position of the patriarch in the $c_i$ clan (best fitness value $x_{best,c_i}$). The clan update operation is

$$x_{new,c_i,j} = x_{c_i,j} + \alpha(x_{best,c_i} - x_{c_i,j})\gamma , \tag{11}$$

where $x_{new,c_i,j}$ is the updated position, $x_{c_i,j}$ is the position of the previous generation, $x_{best,c_i}$ is the position with the best fitness in the $c_i$ clan, $\alpha \in [0,1]$ is a ratio factor representing the degree of influence of the best position of the matriarch $x_{best,c_i}$ on the position of elephant individuals $x_{c_i,j}$ in the clan, and $\gamma \in [0,1]$ is a random number used to increase the diversity of the population in the later stage of the algorithm. The position of the matriarch $x_{best,c_i}$ in the $c_i$ clan is defined as

$$x_{best,c_i,j} = \beta \cdot x_{center,c_i} , \tag{12}$$

where $\beta \in [0,1]$ is the second algorithm parameter dominating the degree of influence on the clan center $x_{center,c_i}$. The clan center is defined as

$$x_{center,c_i,d} = \left(\sum_{j=1}^{n_{c_i}} x_{c_i,j,d}\right) \Big/ n_{c_i} , \tag{13}$$

where $1 \le d \le D$ represents the $d$th dimension, $D$ is the total number of dimensions in the search space, and $n_{c_i}$ is the number of elephants in the $c_i$ clan.

### 4.2 Clan separation operation

The grown-up male elephants will leave their herd to increase the herd's global search capabilities and density. The elephant in the worst position (the elephant with the worst fitness) will be deleted, and a random search will be performed in the search space to increase the search performance.

In each $c_i$ clan, a certain number of elephants with the worst fitness function value will be moved to a new position. Their position is defined as

$$x_{worst,c_i} = x_{\min} + (x_{\max} - x_{\min} + 1) \cdot rand, \tag{14}$$

where $x_{\min}$ and $x_{\max}$ are the lower and upper limits of the search space, respectively; $rand \in [0,1]$.

The basic steps of the EHO algorithm are as follows:

Step 1: Initialize the population and set the maximum number of iterations.

Step 2: Calculate the individual fitness value of each elephant and use the fitness function to obtain the current optimal individual position.

Step 3: Update the individual position of each elephant in the population according to Eq. (11) and the current optimal individual position using Eq. (12).

Step 4: Calculate the individual fitness value of each elephant after the update and evaluate the updated elephant population to obtain the best and worst individual positions in the population.

Step 5: Update the current worst individual position to retain the best solution using Eq. (14).

Step 6: Is the maximum number of iterations reached? If yes, then output the current optimal individual position and the corresponding fitness value; otherwise, return to Step 2.

A block diagram of the proposed MRAC speed prediction DTC PMSM drive using the EHO algorithm to design the adaptation mechanism is shown in Fig. 5, which includes a speed controller, torque controller, flux controller, VSVPWM, torque calculation, stator flux calculation, three-phase system to two-axis stationary frame coordinate transformation ($2^s <= 3$), two-axis stationary to two-axis synchronous frame coordinate transformation ($2^e <= 2^s$), and EHO algorithm MRAC rotor speed prediction scheme based on the reactive power. In this system, P–I-type controllers for the speed, torque, and flux control loops were designed with the pole placement method. The proportional gain ($K_p$), integral gain ($K_i$), damping ratio ($\zeta$), and bandwidth ($BW$) for the three P–I-type controllers are shown in Table 1. The adaptation mechanism of the MRAC rotor speed prediction scheme was designed using the EHO algorithm.

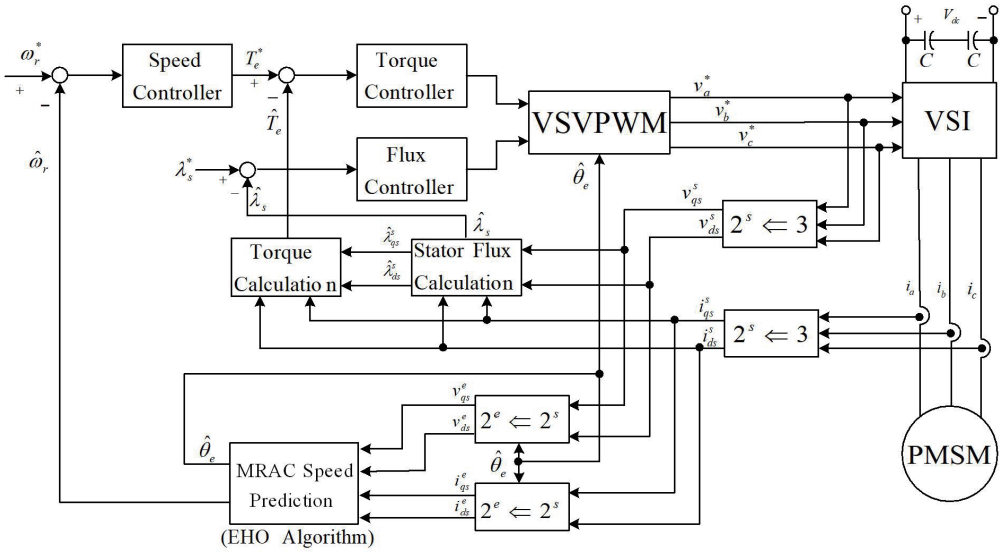


Fig. 5. MRAC speed prediction DTC PMSM drive using the EHO algorithm adaptation scheme.

Table 1
Controller parameters, damping ratio, and bandwidth.

| Controller type | $K_p$ | $K_i$ | $\zeta$ | $BW$ |
|---|---|---|---|---|
| Speed | 3 | 22.5 | 0.741 | 9.77 |
| Torque | 2.07 | 14.3 | 0.712 | 9.03 |
| Flux | 1 | 100 | 0.667 | 141 |

## 5. Experimental Setup and Results

A standard three-phase, 220 V, 0.75 kW, Y-connected PMSM was used to serve as the controlled plant for the simulation and experiment to confirm the effectiveness of the proposed MRAC speed prediction DTC PMSM drive using the EHO algorithm designed as the adaptation mechanism. The simulation system was established using the toolbox MATLAB/Simulink©. The control program was executed using a Texas Instruments DSP 6713-and-F2812 control card. In a running cycle, the speed command was designed as follows: forward direction acceleration from $t = 0$ to $t = 1$ s; forward direction steady-state running at interval $1 \leq t \leq 4$ s; forward direction braking to reach zero speed during $4 \leq t \leq 5$ s; reverse direction acceleration from $t = 5$ to $t = 6$ s; reverse direction steady-state running at interval $6 \leq t \leq 9$ s; and reverse direction braking to reach zero speed during $9 \leq t \leq 10$ s.

The simulated and measured responses with 2 N-m load for a reversible steady-state speed command of 1800 (rev/min) are shown in Figs. 6 and 7. Each figure contains six responses: (a) command (dashed line) and prediction (solid line) rotor speed, (b) command (dashed line) and actual (solid line) rotor speed, (c) electromagnetic torque, (d) stator current, (e) estimated synchronous position angle, and (f) stator flux locus (*q*-axis vs *d*-axis).

From the simulated and measured responses in reversible transient and steady-state operations under a load condition, the proposed MRAC speed prediction DTC PMSM drive can accurately predict the rotor speed. The saw-tooth flux position angle determined the exact coordinate transformation between the synchronous and stationary frames, and the reduction of the electromagnetic torque and stator current ripples was achieved.

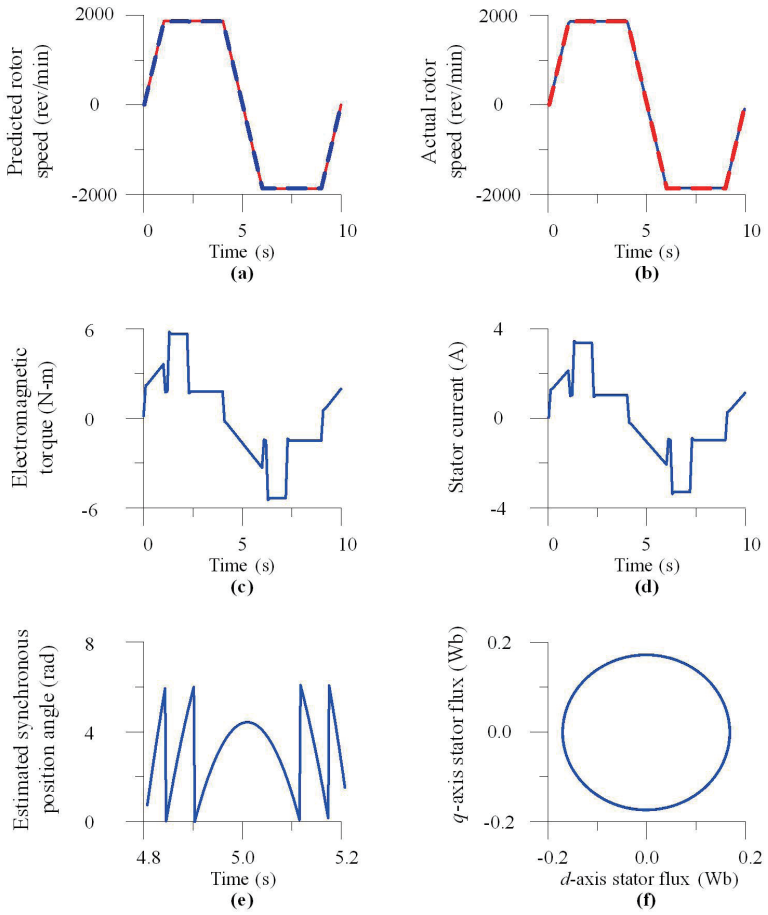


Fig. 6. (Color online) Simulated responses of the MRAC speed prediction DTC PMSM dive using the EHO algorithm designed as the adaptation mechanism with 2 N-m load for the reversible steady-state speed command of 1800 rev/min. (a) Predicted rotor speed, (b) actual rotor speed, (c) electromagnetic torque, (d) stator current, (e) estimated synchronous position angle, and (f) stator flux locus.

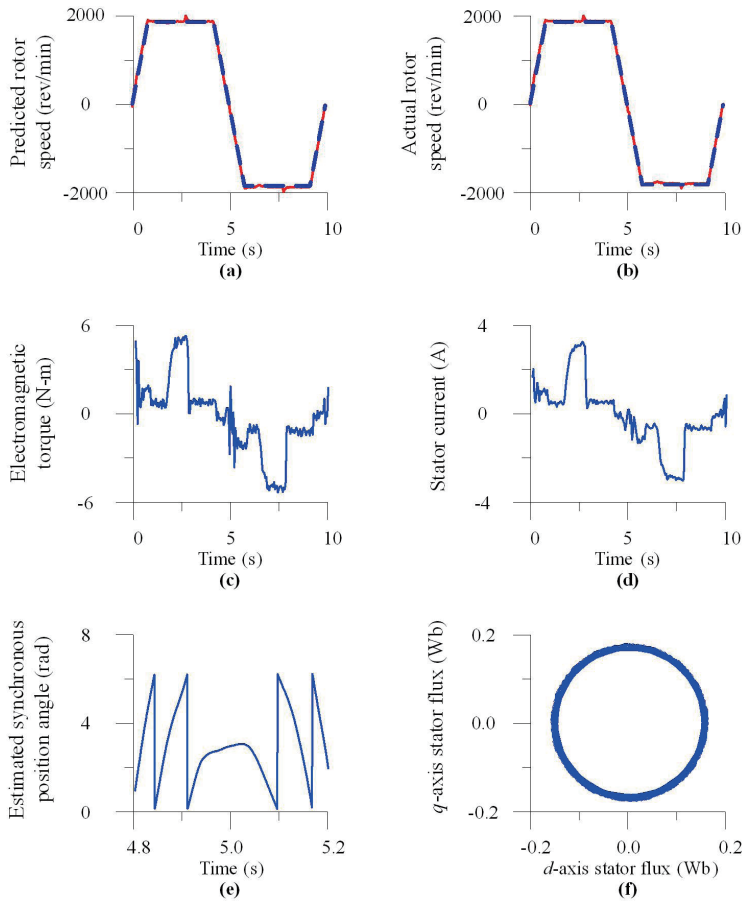


Fig. 7. (Color online) Measured responses of the MRAC speed prediction DTC PMSM dive using the EHO algorithm designed as the adaptation mechanism with 2 N-m load for the reversible steady-state speed command of 1800 rev/min. (a) Predicted rotor speed, (b) actual rotor speed, (c) electromagnetic torque, (d) stator current, (e) estimated synchronous position angle, and (f) stator flux locus.

## 6. Conclusions

An MRAC based on the reactive power using the EHO algorithm designed as the adaptation mechanism was developed for the speed prediction of DTC PMSM drives. The proposed MRAC is based on the reactive power that effectively adjusts the reversible operation speed in the transient and steady states. The saw-tooth synchronous position angle determined the exact coordinate transformation between the synchronous and stationary frames, and the reduction of the electromagnetic torque and stator current ripples was achieved. The stator currents for implementing the MRAC speed prediction of the DTC PMSM drive were provided by Hall effect current sensors. The simulated and measured responses with the load condition for the reversible transient-state and steady-state operations confirm the effectiveness of the proposed approach.

## References


1 Y. Ren, Z. Q. Zhu, and J. Liu: IEEE Trans. Ind. Electron. **61** (2014) 5249. https://doi.org/10.1109/TIE.2014.2300070
2 K. Wang, R. D. Lorenz, and N. A. Baloch: IEEE Trans. Ind. Appl. **54** (2018) 6071. https://doi.org/10.1109/TIA.2018.2855162
3 A. Sarajian, D. A. Khaburi, and M. Rivera: Proc. 2016 7th Power Electronics Drive Systems Technologies Conf. (PEDSTC 2016) 64–69. https://doi.org/10.1109/PEDSTC.2016.7556839
4 A. Y. Talouki, P. Pescetto, G. Pellegrino, and L. Boldea: IEEE Trans. Power Electron. **33** (2018) 2447. https://doi.org/10.1109/TPEL.2017.2697209
5 G. H. B. Foo and M. F. Rahman: IEEE Trans. Pow. Electro. **25** (2010) 933. https://doi.org/10.1109/TPEL.2009.2036354
6 X. Wang, Z. Wang, Z. Xu, M. Cheng, W. Wang, and Y. Hu: IEEE Trans. Power Electron. **34** (2019) 6669. https://doi.org/10.1109/TPEL.2018.2876400
7 M. Nicola, C. L. Nicola, and D. Sacerdotianu: Proc. 2020 21st Int. Sym. Electrical Apparatus & Technologies (SIELA 2020) 1–6. https://doi.org/10.1109/SIELA49118.2020.9167120
8 W. Si and Z. Zhang: Proc. 2017 IEEE Industrial Electronics Society (IECON 2017) 3760–3764. https://doi.org/10.1109/IECON.2017.8216640
9 A. M. Omara, M. Sleptsov, and A. A. Z. Diab: Proc. 2018 25th Int. Workshop Electric Drives: Optimization Control Electric Drives (IWED 2018) 1–6. https://doi.org/10.1109/IWED.2018.8321386
10 S. Sayeef, G. Foo, and M. F. Rahman: IEEE Trans. Ind. Electron. **57** (2010) 3715. https://doi.org/10.1109/TIE.2010.2041730
11 G. D. Andreescu, C. I. Pitic, F. Blaabjerg, and I. Boldea: IEEE Trans. Energy Conv. **23** (2008) 393. https://doi.org/10.1109/TEC.2007.914386
12 D. Nguyen, R. Dutta, and M. F. Rahman: Proc. 2013 IEEE Power Electronics Drive System (PEDS 2013) 1312–1317. https://doi.org/10.1109/PEDS.2013.6527222
13 Z. Xu and M. F. Rahman: IEEE Trans. Ind. Electron. **59** (2012) 4179. https://doi.org/10.1109/TIE.2012.2188252
14 G. Foo and M. F. Rahman: IEEE Trans. Ind. Electron. **57** (2009) 395. https://doi.org/10.1109/TIE.2009.2030815
15 M. Moradian, J. Soltani, A. N. Khodabakhsh, and G. R. A. Markadeh: IEEE Trans. Ind. Inform. **15** (2018) 205. https://doi.org/10.1109/TII.2018.2808521
16 B. Singh, B.P. Singh, and S. Dwivedi: Proc. 2006 IEEE Int. Industrial Technology Conf. (ICIT 2006) 1301–1308. https://doi.org/10.1109/ICIT.2006.372403
17 C. H. Liu: Control of AC Electrical Machines (Tunghua, Taipei, 2008) 4th ed., Chap. 2 (in Chinese).
18 C. W. Secrest, J. S. Pointer, M. R. Buehner, and R. D. Lorenz: IEEE Trans. Ind. Appl. **51** (2015) 4492. https://doi.org/10.1109/TIA.2015.2443100
19 G. G. Wang, S. Deb, and L. S. Coelho: Proc. 2015 3rd Int. Computational and Business Intelligence Symp. (ISCBI 2015) 1–5. https://doi.org/10.1109/ISCBI.2015.8
20 J. Li, H. Lei, A. H. Alavi, and G. G. Wang: Math. **8** (2020) 1. https://doi.org/10.3390/math8091415
21 S. M. Almufti, R. R. Asaad, and B. W Salim: Engi. Tech. **7** (2018) 6109. https://doi.org/10.14419/ijet.v7i4.23127